The Cryosphere Discuss., https://doi.org/10.5194/tc-2018-228
Manuscript under review for journal The Cryosphere
Discussion started: 29 November 2018

The Cryosphere Discussions
Open Access
EGU

Submarine melt as a potential trigger of the NEGIS margin retreat during MIS-3.

Ilaria Tabone[1,2], Alexander Robinson[1,2,3], Jorge Alvarez-Solas[1,2], and Marisa Montoya[1,2]

[1]Universidad Complutense de Madrid, 28040 Madrid, Spain
[2]Instituto de Geociencias, Consejo Superior de Investigaciones Cientificas-Universidad Complutense de Madrid, 28040 Madrid, Spain
[3]Now at Faculty of Geology and Geoenvironment, University of Athens, 15784 Athens, Greece

Correspondence to: Ilaria Tabone (itabone@ucm.es)

Abstract. The Northeast Greenland Ice Stream (NEGIS) area has been suffering a significant ice mass loss during the last decades. This is partly due to increasing oceanic temperatures in the subpolar North Atlantic, which enhance submarine basal melting and mass discharge. This demonstrates the high sensitivity of this region to oceanic changes. Alongside, a recent study suggests that the NEGIS grounding line was 20-40 km behind its present-day location for 15 ka during Marine Isotopic Stage (MIS) 3, raising an important conundrum. This retreat has been attributed to a combination of atmospheric and external forcings but a modelling approach to the problem is pending. Here we investigate the sensitivity of the NEGIS to the oceanic forcing during the Last Glacial Period (LGP) using a three-dimensional hybrid ice-sheet-shelf model. We find that a sufficiently high oceanic forcing could account for a NEGIS ice-margin retreat of several tens of km, potentially explaining the recently proposed NEGIS grounding-line retreat during MIS-3.

1 Introduction

The Northeast Greenland Ice Stream (NEGIS) is the largest ice stream in the Greenland Ice Sheet (GrIS), extending more than 600 km inland (Joughin et al., 2001) and discharging 12 % of the whole ice sheet through three outlet glaciers (Rignot and Mouginot, 2012): Nioghalvfjerdsfjord Gletscher (NG), Zachariae Isstrøm (ZI), and Storstrømmen Gletscher (SG), which is today a surging glacier. These marine-terminating glaciers have suffered huge changes in the last decades. ZI retreated and almost lost its remaining ice shelf after more than a decade of enhanced ice mass loss, increasing its speed by 50 % in less than 15 years (Mouginot et al., 2015). Although NG seems to be more stable than ZI due to its bed configuration, it has lost mass since 2001 (Mayer et al., 2018), with peaks of speedup during 2016 (Rathmann et al., 2017). Ice loss from these two marine-terminating glaciers is thought to be partly related to the increasing temperature of North Atlantic waters (Khan et al., 2014; Mouginot et al., 2015), which increases the oceanic heat flux and accelerates the submarine melting (Mayer et al., 2018). This hypothesis is supported by the three-decade-long observed warming in the subpolar North Atlantic (Straneo and

Heimbach (2013) and references therein). Moreover, warmer oceanic waters in Fram Strait could directly reach the NG, further increasing its basal melting and potentially causing the loss of its floating ice tongue (Schaffer et al., 2017). A recent study investigating the response of NG and ZI to oceanic forcing with the aim of constraining their future stability suggests a further slow retreat of NG and a complete loss of the ZI ice tongue due to increasing melt rates in the next decades (Choi et al., 2017) but these conclusions could be even too conservative (Larsen et al., 2018).

Reconstructions suggest that during the Last Glacial Maximum (LGM), ca. 21 ka Before Present (BP), the northeastern region of the GrIS considerably advanced, likely reaching the continental shelf break, at 250-300 km from the present-day coastline (Arndt et al., 2015, 2017; Winkelmann et al., 2010). Although the age of these LGM reconstructions is still poorly constrained, the combination of cosmogenic exposure and radiocarbon dating has recently facilitated the reconstruction of the position of the NEGIS further back in time, over the last 45 ka (Larsen et al., 2018). This study suggests that the ice margin largely fluctuated throughout this period, even retreating by 70 km behind its present-day position during the mid-Holocene (ca. 7-5 ka BP) and by 20-40 km during part of Marine Isotopic State (MIS) 3, ca. 60-25 ka BP. The Holocene retreat was likely due to an increase in both atmospheric and oceanic temperatures comparable to that of today or expected for the near future. On the other hand, the retreat during MIS-3 was attributed to a combination of atmospheric and external forcings but no ice-sheet modelling study was undertaken yet to corroborate this conclusion. In addition, the potential role of oceanic forcing in this retreat has not been explicitly investigated. In the light of the ongoing changes in the GrIS attributed to ice-ocean interactions, this appears as a plausible mechanism that needs to be investigated.

Here we use an ice-sheet-shelf model to investigate the sensitivity of the NEGIS grounding line to changing oceanic conditions during the last glacial period (LGP). The submarine melting at the grounding line is parameterised in such a way that basal melt is allowed during relatively warm time periods such as the present, the last interglacial (LIG, ca. 130-115 ka BP) or MIS-3, whereas it reaches zero at the onset of the LGM. We study the NEGIS marine margin response to increasing basal melting rates during MIS-3 to show that a sufficiently high oceanic sensitivity could have driven a considerable NEGIS grounding-line retreat during MIS-3 from its former glacial position.

2 Methods

To simulate the NEGIS response to past oceanic forcing, we use the three-dimensional, hybrid ice-sheet-shelf model GRISLI-UCM (Alvarez-Solas et al., 2018; Tabone et al., 2018), adapted from the extensively used GRISLI model (Ritz et al., 2001). Grounded, slow-moving ice-sheet regions and floating shelves are treated through the shallow-ice approximation (SIA) and shallow-shelf approximation (SSA), respectively. In the transition between these two regimes (i.e., fast moving, grounded ice), the dynamics is solved by the simple addition of the SIA and SSA velocity solutions (Winkelmann et al., 2011). The SSA boundary condition is provided by basal sliding below the ice streams following a friction law, in which the basal shear stress is proportional to the basal velocity and to a sliding coefficient dependent on the effective pressure at the bed. Glacial isostatic adjustment of the bedrock due to variations in the ice load is reproduced through the Elastic Lithosphere Relaxing Asthenosphere model (Greve and Blatter, 2009). Unlike some recent hybrid models, the grounding-line position is defined

The Cryosphere Discuss., https://doi.org/10.5194/tc-2018-228
Manuscript under review for journal The Cryosphere
Discussion started: 29 November 2018

through a pure flotation criterion involving ice thickness at the marine margin and prescribed sea level. Calving occurs whenever a two-constraint thickness rule is satisfied at the ice-ocean interface (Colleoni et al., 2014): first, the ice-front thickness must be lower than a fixed threshold (H=200 m here); second, the upstream ice advection does not succeed in preserving the ice-front thickness above that threshold.

The atmospheric temperature forcing applied to the model follows an anomaly method according to which the present-day climatological temperature $T_{\mathrm{clim,atm}}$ is perturbed by past anomalies obtained from a spatially-uniform proxy-derived index $\alpha(t)$:

$$T_{\mathrm{atm}}(t) = T_{\mathrm{clim,atm}} + (1-\alpha(t))(T_{\mathrm{LGM,atm}} - T_{\mathrm{PD,atm}}) \quad (1)$$

The α(t) index is derived from the Greenland temperature reconstruction for the Holocene (Vinther et al., 2009), the North Greenland Ice Core Project (NGRIP) reconstruction for the LGP (Kindler et al., 2014) and the North Greenland Eemian Ice Drilling (NEEM) reconstruction for the LIG (NEEM, 2013), as in Tabone et al. (2018). The composed signal is then smoothed so that the spectral components below orbital frequencies are removed (i.e., periods below 16 ka). By construction, $\alpha = 1$ at present day (PD) and $\alpha = 0$ at the LGM. $T_{\mathrm{clim,atm}}$ is taken from the regional climate model MAR forced by ERA-Interim (Fettweis et al., 2013), averaged over years 1981-2010. $T_{\mathrm{LGM,atm}} - T_{\mathrm{PD,atm}}$ is the glacial minus interglacial atmospheric temperature anomaly simulated by the climate model of intermediate complexity CLIMBER-3α (Montoya and Levermann, 2008). The precipitation field is obtained following a similar approach based on the ratio of LGM and present-day precipitation, scaled by α (Banderas et al., 2018):

$$P_{\mathrm{ann}}(t) = P_{\mathrm{clim,ann}} \cdot \left(\alpha(t) + (1-\alpha(t)) \cdot \frac{P_{\mathrm{LGM,ann}}}{P_{\mathrm{PD,ann}}} \right). \quad (2)$$

Surface ablation is calculated by the simple positive degree (PDD) scheme (Reeh, 1989). Although this scheme does not account for past insolation changes, here we primarily assess the sensitivity of the NEGIS to the oceanic forcing during glacial times. Therefore, we expect that the choice of the surface melt model should not jeopardise our results.

The oceanic forcing is prescribed at the grounding line through a parameterisation of the submarine melt rate based on an anomaly method for which the present-day melt rate is perturbed by its past changes associated with variations in the oceanic temperature (Tabone et al., 2018):

$$B_{\mathrm{m}}(t) = B_{\mathrm{ref}} + \kappa \Delta T_{\mathrm{ocn}}(t) \quad (3)$$

where $B_{\mathrm{m}}(t)$ is the melt rate at the grounding line at a given time ($m\ a^{-1}$), B_{ref} is the present-day basal melting rate at the grounding line ($m\ a^{-1}$) and κ is a coefficient representing the heat-flux exchanged between water and ice at the ice-ocean front ($m\ a^{-1}\ K^{-1}$). Past oceanic temperatures below the ice ($\Delta T_{\mathrm{ocn}}(t)$) evolve as:

$$\Delta T_{\mathrm{ocn}}(t) = (1-\alpha(t))(T_{\mathrm{LGM,ocn}} - T_{\mathrm{PD,ocn}}) \quad (4)$$

where the $\alpha(t)$ index is that of Eq. 1 and $T_{\mathrm{LGM,ocn}} - T_{\mathrm{PD,ocn}}$ is the glacial minus interglacial oceanic temperature anomaly (K). The system of equations 3-4 can be solved assigning values to B_{ref}, κ, $T_{\mathrm{LGM,ocn}}$ and $T_{\mathrm{PD,ocn}}$. However, some simplifications can be considered during the parameter assignment. Following Tabone et al. (2018), the reference melting rate B_{ref} is

The Cryosphere Discuss., https://doi.org/10.5194/tc-2018-228
Manuscript under review for journal The Cryosphere
Discussion started: 29 November 2018

proportional to the oceanic sensitivity κ, as it is defined as

$$B_{\mathrm{ref}} = \kappa(T_{\mathrm{clim,ocn}} - T_f). \quad (5)$$

$T_{\mathrm{clim,ocn}}$ is the climatological mean of the oceanic temperature considered at the grounding-line depth (K) and T_f is the freezing point temperature at the grounding line (K). The former is depth-dependent; the latter also depends on the distribution of salinity in the water column. Introducing B_{ref} in the equation is a simplification made to avoid the choice of values to be assigned to these two variables, that might be challenging and unconstrained (Beckmann and Goosse, 2003). For the sake of simplicity, $T_{\mathrm{clim,ocn}} - T_f$ can be considered as spatially (horizontally and vertically) constant, in the way that B_{ref} is defined to scale directly with κ. Here, we prescribe $T_{\mathrm{clim,ocn}} - T_f$ = 1 K, thus $B_{\mathrm{ref}} = \kappa \cdot 1$ K. Also, the glacial-interglacial temperature anomaly $T_{\mathrm{LGM,ocn}} - T_{\mathrm{PD,ocn}}$ is considered here to be spatially uniform and set to a value of -1 K (Annan and Hargreaves, 2013; MARGO, 2009). With these simplifications, the system of Eq. 3-4 is thus reduced to a problem of one degree of freedom (κ). Investigated values of κ range from 0 to 10 $m\ a^{-1}\ K^{-1}$; thus B_{ref} ranges from 0 to 10 $m\ a^{-1}$. These κ values are consistent with the inference from the Antarctic Ice Sheet that a change of 1 K in the oceanic temperature varies the melt rate by 10 $m\ a^{-1}$ (Rignot and Jacobs, 2002). Moreover, the resulting B_{ref} values are in the range of the submarine melt observed at the grounding line of PD Greenland glaciers that have floating ice shelves (Wilson et al., 2017). Melting at the base of the ice shelves is defined to be the 10% of that calculated at the grounding line which reflects the decrease of melting rate observed towards the ice shelves (Münchow et al., 2014; Rignot and Steffen, 2008; Wilson et al., 2017). However, this decrease is not parameterised here as a function of the distance from the grounding line. Instead, submarine melt is here assumed to have a binary behavior: it is equal to B_m at the grounding line and to the 10% of B_m at all floating grid cells. Since the submarine melting rate at the grounding line is calculated to be spatially constant along the whole domain, the resulting value of the sub-shelf melt rate is also spatially uniform and is shared by all the ice-shelf grid cells of the domain. Note that refreezing below the grounding line is not allowed and it is cut off to zero, thus there is neither melting nor refreezing during the LGM for the whole set of experiments. The spectrum of resulting submarine melt rates leads to 11 different submarine melt configurations, for which an increase in the oceanic sensitivity entails an increase of the melting rate during MIS-3 (Fig. 2). These configurations allow investigating the role of the submarine melting rate on the NEGIS margin position during the LGP. Model simulations of the whole GrIS are initialized at 250 ka BP using the PD GrIS topography from Schaffer et al. (2016) and run under transient climatic conditions for two full glacial cycles with a horizontal resolution of 10 km. The first glacial cycle has been considered as a spin up. The analysis of the results focuses on the NEGIS sector.

3 Results

The experiment with submarine melt prescribed to zero ($\kappa = 0$, $B_{\mathrm{ref}} = 0$), which is hereafter referred to as the unperturbed experiment, shows the NEGIS margin rapidly advancing towards the continental shelf during glacial inception (Fig. 1). In less than 20 ka after the peak of the Eemian, the grounding line advances through the inner sector of the continental shelf, extending offshore to a distance of about 250 km from the PD NEGIS margin already at around 70 ka BP. During MIS-3, the ice-margin

The Cryosphere Discuss., https://doi.org/10.5194/tc-2018-228
Manuscript under review for journal The Cryosphere
Discussion started: 29 November 2018

position remains substantially steady. The maximum extension of the NEGIS is reached during the LGM, when the ice sheet becomes grounded slightly further offshore (about 20 km) reducing the area of the floating ice shelf in the region (Fig 3 a-e).

In all other simulations, the ocean forcing is switched on ($\kappa, B_{\mathrm{ref}} > 0$) and intensifies for increasing κ (Fig. 2). The location of the grounding line at the LIG is the same in all simulations and thus insensitive to κ, and set mainly by the atmospheric forcing. Another common feature of these simulations is the response of the grounding-line position right after the peak of the Eemian (Fig. 1): the inclusion of positive melt rates before 70 ka BP somewhat constrains the NEGIS margins between 200-300 km upstream of the grounding-line position obtained for the unperturbed experiment, close to its location at the LIG. At about 70 ka BP, the ice margin starts to advance towards the continental shelf break, reaching the minimum LGM grounding-line position estimate based on reconstructions (Funder et al., 2011) in 5-10 ka.

The strongest reaction of the NEGIS grounding line to the applied submarine melting rate is found during MIS-3, when increasing the oceanic forcing not only helps to preclude the grounding-line advance (as compared to the unperturbed case with no oceanic forcing) but furthermore triggers its retreat. By including a basal melt rate of $0 - 0.5\ m\ a^{-1}$ ($\kappa = 1\ m\ a^{-1}\ K^{-1}$), during MIS-3 the location of the NEGIS margin moves 100 km further inland with respect to the unperturbed experiment. Increasing the submarine melt up to $0 - 1.2\ m\ a^{-1}$ ($\kappa = 4\ m\ a^{-1}\ K^{-1}$) not only helps to constrain the NEGIS advance towards the continental shelf after glacial inception (ca. 115 ka BP), but subsequently triggers a slight grounding-line retreat inland by 80 km more which culminates at around 40 ka BP. A higher oceanic sensitivity ($\kappa = 5\ m\ a^{-1}\ K^{-1}$) leads to a further and earlier retreat during MIS-3. The minimum extent of grounded ice during MIS-3 is reached around 45 ka BP, when the grounding line retreats by more than 100 km inland from its position simulated at 60 ka BP. The ice margin then remains steady until the end of MIS-3 (Fig. 1). This value of κ and the resulting basal melt configuration (MIS-3 values above $1.6\ m\ a^{-1}$) act as a threshold above which the submarine melt rate forces the grounding line to retreat by several km inland during MIS-3. For higher basal melt rates the grounding line retreats further inland, stationing at only 30-40 km far from the PD position.

The effect of the submarine melt rate applied to the NEGIS marine margin during MIS-3 is also perceived far inland. The basal melt imposed at the ice-ocean interface (region B) causes the ice margin to retreat inland, strongly enhancing ice discharge (Fig. 4). The reduction of buttressing previously ensured by the presence of ice on the continental shelf increases margin velocities, which propagate inland (Fig. 3 f), causing a decrease of ice thickness in the ice-sheet interior (region A). An initial strong peak in ice discharge is observed, following the initial increase of submarine melting and loss of buttressing, but the effect persists with further ice discharge until the end of MIS-3. At this moment, the absence of melt imposed through the LGM allows the grounding line to advance again towards the continental shelf break (Fig. 3 g-j). The maximum distance reached at the peak of the LGM and the time of the onset of the advance are inversely proportional to the melt rate suffered in the previous millennia (Fig. 2). A strong melt rate imposed during MIS-3 leads to a delayed triggering and spatially-constrained grounding-line advance, and vice versa.

By construction, submarine melt occurs again after 20 ka BP, when both atmospheric and oceanic temperatures increase, contributing to push the grounding line back towards the ice-sheet interior (Fig. 1). The fact that the unperturbed experiment simulates this retreat as well demonstrates that it is driven by both increasing atmospheric and oceanic temperatures during the Holocene. Nevertheless, the presence of submarine melt at the NEGIS marine margins enhances the retreat and triggers

The Cryosphere Discuss., https://doi.org/10.5194/tc-2018-228
Manuscript under review for journal The Cryosphere
Discussion started: 29 November 2018

it slightly earlier. However, this feature saturates for high values of B_{ref}, as a further retreat inland is constrained by the bathymetry.

4 Discussion

The NEGIS grounding-line fluctuations simulated in response to a high oceanic forcing in this set of experiments are similar to those suggested by Larsen et al. (2018) for the last 45 ka. However, there are some major differences between our results and theirs that deserve further attention.

First, we do not simulate the MIS-3 retreat farther inland than the PD position (20-40 km), although our simulations do show a retreat of more than 100 km with respect to the previous millennia. This MIS-3 retreat behind the PD NEGIS margin position has been attributed by Larsen et al. (2018) to lower accumulation rates, high incoming solar radiation and increasing summer air temperatures operating together. Since we have not investigated the sensitivity to these forcings separately and our experiments do not show this extended retreat, we can neither confirm nor discard their hypothesis. However, our work has demonstrated that the presence of relatively high submarine melt rates at the NEGIS grounding line during MIS-3 is enough to cause a substantial retreat of its marine margins during this period.

Second, our simulated grounding-line advance during the LGM is smaller than the maximum extension suggested by reconstructions (Funder et al., 2011). This bias furthermore increases with increasing oceanic forcing. However, even in the unperturbed experiment, which allows the largest ice-sheet expansion due to the absence of melting at the marine margins, the grounding line does not reach the continental shelf break either. This could be related to model dynamics, such as insufficient basal drag imposed at the base of the ice streams or the ice velocity mixing in transition zones, or simplified boundary conditions.

Third, the timings of the grounding-line advance/retreat for the last 35 ka of the LGP do not precisely correspond to those proposed by Larsen et al. (2018). In the experiments that show a significant retreat during MIS-3 ($\kappa > 4\ m\ a^{-1}\ K^{-1}$), we simulate both the grounding-line advance at the end of this stage and the retreat at the onset of the Holocene earlier than expected. This is due to the submarine melting signal representing oceanic temperature anomalies, which saturates at around 35 ka BP and is switched on again at 20 ka BP, assuming that the LGM starts and ends at these times. By using the same α for both atmospheric and oceanic forcing, we are assuming the evolution of the ocean around Greenland at orbital timescales to be comparable to that of the climate. This is a simple assumption, but reasonable due to the lack of clear information from climate proxies. However, any uncertainty in the orbital forcing affects the ice-sheet retreat during the Holocene which is supposed to be a combination of atmospheric and oceanic temperatures (Larsen et al., 2018). The Holocene maximum is quite well reproduced in our submarine melting configurations (Fig. 2) and in the atmospheric temperature evolution. However, the slight basal melt decrease applied in the late Holocene is not sufficient to make the grounding line advance back towards the continental borders and the inaccurate position simulated at the PD is a direct consequence of this simplification.

The grounding-line retreat at the PD is proportional to the magnitude of the submarine melt rate imposed at the NEGIS ice margins during the mid-late Holocene, which is related to the value of B_{ref} used. However, this correspondence is very weak

and the retreat quickly saturates at about 50 km away from the PD position for increasing κ. Although this retreat is supported by proxies for the mid-Holocene (Bennike and Weidick, 2001; Larsen et al., 2018), its persistence until the present day is unrealistic. Estimated PD grounding-line melt rates at 79°N reach peaks of $50\ m\ a^{-1}$, which are even higher than the B_{ref} values considered in this work (Wilson et al., 2017). Imposing these would likely cause a farther retreat inland. This bias found in our experiments could be related to the low spatial resolution of the model (10 km) which does not allow for a precise treatment of the grounding-line zone and may trigger nonlinear effects, enhancing grounding-line retreat farther inland than expected. Another factor affecting this extended PD retreat is related to the design of the submarine melt signal itself during the Holocene, which shows a constant increase from 0 to the set B_{ref} value through the last 20 ka. Peaks of up to $50\ m\ a^{-1}$ occur at the NEGIS margin, however it is unlikely that this could have happened for a long period of time and in such a persistent way. This continuous and spatially-extended melt increase contributes to enhance the retreat at the PD by several km.

The oceanic forcing is defined here to be in phase with the atmospheric forcing, as they are both set to evolve in time through the same NGRIP-derived index α. To our knowledge, little evidence on oceanic changes at orbital timescales is available and whether the best representation of reality would be through oceanic temperatures varying in phase or antiphase with the atmosphere is unknown. Nevertheless, proxy-based temperature reconstructions indicate glacial-interglacial surface temperature anomalies to be between 0 and -3 K (Annan and Hargreaves, 2013; MARGO, 2009) and the value chosen for $T_{\mathrm{LGM,ocn}} - T_{\mathrm{PD,ocn}}$ is within this range (-1 K).

This work represents the first attempt to simulate the striking margin retreat reconstructed for the NEGIS during MIS-3 (Larsen et al., 2018). Here we have shown that the orbitally-driven oceanic warming during MIS-3 is sufficient to explain the retreat of the NEGIS grounding line during part of the LGP. Nevertheless, the rapid occurrence of warm oceanic pulses on millennial timescales is an important characteristic of MIS-3. Given the non-linear response of subglacial melting to temperature variations (e.g. Mikkelsen et al. (2018)), this effect could potentially modulate the orbitally-driven response on shorter timescales. A complete treatment of the problem from this perspective is difficult, however, by the absence of reconstructions of the oceanic conditions of the northeastern part of Greenland on these timescales during MIS-3.

In addition, such a retreat of the ice margin may have triggered feedbacks on the local climate that are not taken into account in this work. For example, it is possible that this large ice retreat would have caused changes in the albedo, affecting surface air temperatures and snow accumulation. Other feedbacks related to the freshwater flux into the ocean could have led to variations in sea ice and local oceanic circulation. All these processes, not included here, could have additionally contributed to variations in the ice thickness and grounding-line position, and should be investigated in the future for a complete understanding of the conundrum.

5 Conclusions

We have studied the sensitivity of the NEGIS ice margin to oceanic forcing during the LGP. To this end, we used a three-dimensional, hybrid ice-sheet-shelf model in which the submarine melt rate is parameterised to perform simulations of the GrIS for which basal melt follows a ice-core-proxy-derived curve assumed to represent the evolution of both atmospheric and

oceanic temperatures at orbital scales. The increase in basal melt during MIS-3 reflects a relatively warm oceanic state, whereas the lack of basal melt during the LGM corresponds to the associated expected minimum in oceanic temperatures. We showed that in the absence of submarine melting during the entire LGP, the grounding line advances towards the continental shelf just after the LIG. On the other hand, switching on the oceanic forcing helps to constrain the ice margin advance during MIS-3. Sufficiently high submarine melt rates eventually trigger its retreat by more than 100 km from its former position. The lack of basal melt during the LGM then resumes the grounding-line advance by 200 km towards the continental shelf break. Our results robustly show that a prolonged presence of submarine melt at the NEGIS ice margin is enough to substantially contribute to grounding-line retreat there, which helps to explain the recently suggested NEGIS ice margin retreat during MIS-3.

The Cryosphere Discuss., https://doi.org/10.5194/tc-2018-228
Manuscript under review for journal The Cryosphere
Discussion started: 29 November 2018

References

Alvarez-Solas, J., Banderas, R., Robinson, A., , and Montoya, M.: Oceanic forcing of the Eurasian Ice Sheet on millennial time scales during the Last Glacial Period, Clim. Past Discuss., 2018.

Annan, J. D. and Hargreaves, J. C.: A new global reconstruction of temperature changes at the Last Glacial Maximum, Climate of the Past, 9, 367–376, 2013.

Arndt, J. E., Jokat, W., Dorschel, B., Myklebust, R., Dowdeswell, J. A., and Evans, J.: A new bathymetry of the Northeast Greenland continental shelf: Constraints on glacial and other processes, Geochemistry, Geophysics, Geosystems, 16, 3733–3753, 2015.

Arndt, J. E., Jokat, W., and Dorschel, B.: The last glaciation and deglaciation of the Northeast Greenland continental shelf revealed by hydro-acoustic data, Quaternary Science Reviews, 160, 45–56, 2017.

Banderas, R., Alvarez-Solas, J., Robinson, A., and Montoya, M.: A new approach for simulating the paleo-evolution of the Northern Hemisphere ice sheets, Geoscientific Model Development, 11, 2299–2314, 2018.

Beckmann, A. and Goosse, H.: A parameterization of ice shelf-ocean interaction for climate models, Ocean Modelling, 5, 157–170, 2003.

Bennike, O. and Weidick, A.: Late Quaternary history around Nioghalvfjerdsfjorden and Jøkelbugten, North-East Greenland, Boreas, 30, 205–227, 2001.

Choi, Y., Morlighem, M., Rignot, E., Mouginot, J., and Wood, M.: Modeling the response of Nioghalvfjerdsfjorden and Zachariae Isstrøm Glaciers, Greenland, to ocean forcing over the next century, Geophysical Research Letters, 44, 2017.

Colleoni, F., Masina, S., Cherchi, A., Navarra, A., Ritz, C., Peyaud, V., and Otto-Bliesner, B.: Modeling Northern Hemisphere ice-sheet distribution during MIS 5 and MIS 7 glacial inceptions, Climate of the Past, 10, 269–291, 2014.

Fettweis, X., Franco, B., Tedesco, M., Van Angelen, J., Lenaerts, J., Van den Broeke, M., and Gallée, H.: Estimating Greenland ice sheet surface mass balance contribution to future sea level rise using the regional atmospheric climate model MAR, The Cryosphere, 7, 469–489, 2013.

Funder, S., Kjeldsen, K. K., Kjær, K. H., and Cofaigh, C. Ó.: The Greenland Ice Sheet during the past 300,000 years: A review, in: Developments in Quaternary Sciences, vol. 15, pp. 699–713, 2011.

Greve, R. and Blatter, H.: Dynamics of ice sheets and glaciers, Springer Science & Business Media, 2009.

Joughin, I., Fahnestock, M., MacAyeal, D., Bamber, J. L., and Gogineni, P.: Observation and analysis of ice flow in the largest Greenland ice stream, Journal of Geophysical Research: Atmospheres, 106, 34 021–34 034, 2001.

Khan, S. A., Kjær, K. H., Bevis, M., Bamber, J. L., Wahr, J., Kjeldsen, K. K., Bjørk, A. A., Korsgaard, N. J., Stearns, L. A., Van Den Broeke, M. R., et al.: Sustained mass loss of the northeast Greenland ice sheet triggered by regional warming, Nature Climate Change, 4, 292, 2014.

Kindler, P., Guillevic, M., Baumgartner, M., Schwander, J., Landais, A., and Leuenberger, M.: Temperature reconstruction from 10 to 120 kyr b2k from the NGRIP ice core, Clim. Past, 10, 887–902, 2014.

Larsen, N. K., Levy, L. B., Carlson, A. E., Buizert, C., Olsen, J., Strunk, A., Bjørk, A. A., and Skov, D. S.: Instability of the Northeast Greenland Ice Stream over the last 45,000 years, Nature communications, 9, 1872, 2018.

MARGO, P. m.: Constraints on the magnitude and patterns of ocean cooling at the Last Glacial Maximum, Nat. Geosci., 2, 127–132, 2009.

Mayer, C., Schaffer, J., Hattermann, T., Floricioiu, D., Krieger, L., Dodd, P. A., Kanzow, T., Licciulli, C., and Schannwell, C.: Large ice loss variability at Nioghalvfjerdsfjorden Glacier, Northeast-Greenland, Nature communications, 9, 2768, 2018.

Mikkelsen, T. B., Grinsted, A., and Ditlevsen, P.: Influence of temperature fluctuations on equilibrium ice sheet volume, The Cryosphere, 12, 39–47, 2018.

Montoya, M. and Levermann, A.: Surface wind-stress threshold for glacial Atlantic overturning, Geophys. Res. Lett., 35, L03 608, 2008.

Mouginot, J., Rignot, E., Scheuchl, B., Fenty, I., Khazendar, A., Morlighem, M., Buzzi, A., and Paden, J.: Fast retreat of Zachariæ Isstrøm, northeast Greenland, Science, 350, 1357–1361, 2015.

Münchow, A., Padman, L., and Fricker, H. A.: Interannual changes of the floating ice shelf of Petermann Gletscher, North Greenland, from 2000 to 2012, Journal of Glaciology, 60, 489–499, 2014.

NEEM: Eemian interglacial reconstructed from a Greenland folded ice core, Nature, 493, 489–494, 2013.

Rathmann, N., Hvidberg, C., Solgaard, A., Grinsted, A., Gudmundsson, G. H., Langen, P. L., Nielsen, K., and Kusk, A.: Highly temporally resolved response to seasonal surface melt of the Zachariae and 79N outlet glaciers in northeast Greenland, Geophysical Research Letters, 44, 9805–9814, 2017.

Reeh, N.: Parameterization of melt rate and surface temperature on the Greenland ice sheet, Polarforschung, 59, 113–128, 1989.

Rignot, E. and Jacobs, S. S.: Rapid bottom melting widespread near Antarctic Ice Sheet grounding lines, Science, 296, 2020–2023, 2002.

Rignot, E. and Mouginot, J.: Ice flow in Greenland for the international polar year 2008–2009, Geophysical Research Letters, 39, 2012.

Rignot, E. and Steffen, K.: Channelized bottom melting and stability of floating ice shelves, Geophysical Research Letters, 35, L02 503, 2008.

Ritz, C., Rommelaere, V., and Dumas, C.: Modeling the evolution of Antarctic Ice Sheet over the last 420,000 years. Implications for altitude changes in the Vostok region, J. Geophys. Res., 106(D23), 31 943–31 964, 2001.

Schaffer, J., Timmermann, R., Arndt, J. E., Kristensen, S. S., Mayer, C., Morlighem, M., and Steinhage, D.: A global, high-resolution data set of ice sheet topography, cavity geometry, and ocean bathymetry., Earth Systm Scientific Data, 8, 543–557, 2016.

Schaffer, J., von Appen, W.-J., Dodd, P. A., Hofstede, C., Mayer, C., de Steur, L., and Kanzow, T.: Warm water pathways toward Nioghalvfjerdsfjorden Glacier, northeast Greenland, Journal of Geophysical Research: Oceans, 122, 4004–4020, 2017.

Straneo, F. and Heimbach, P.: North Atlantic warming and the retreat of Greenland's outlet glaciers, Nature, 504, 36–43, https://doi.org/10.1038/nature12854, 2013.

Tabone, I., Blasco, J., Robinson, A., Alvarez-Solas, J., and Montoya, M.: The sensitivity of the Greenland Ice Sheet to glacial–interglacial oceanic forcing, Climate of the Past, 14, 455–472, 2018.

Vinther, B. M., Buchardt, S. L., Clausen, H. B., Dahl-Jensen, D., Johnsen, S. J., Fisher, D., Koerner, R., Raynaud, D., Lipenkov, V., Andersen, K., et al.: Holocene thinning of the Greenland ice sheet, Nature, 461, 385–388, 2009.

Wilson, N., Straneo, F., and Heimbach, P.: Submarine melt rates and mass balance for Greenland's remaining ice tongues, The Cryosphere Discuss., pp. 1–17, 2017.

Winkelmann, D., Jokat, W., Jensen, L., and Schenke, H.-W.: Submarine end moraines on the continental shelf off NE Greenland–Implications for Lateglacial dynamics, Quaternary Science Reviews, 29, 1069–1077, 2010.

Winkelmann, R., Martin, M. A., Haseloff, M., Albrecht, T., Bueler, E., Khroulev, C., and Levermann, A.: The Potsdam parallel ice sheet model (PISM-PIK)–Part 1: Model description, The Cryosphere, 5, 715–726, 2011.

The Cryosphere Discuss., https://doi.org/10.5194/tc-2018-228
Manuscript under review for journal The Cryosphere
Discussion started: 29 November 2018

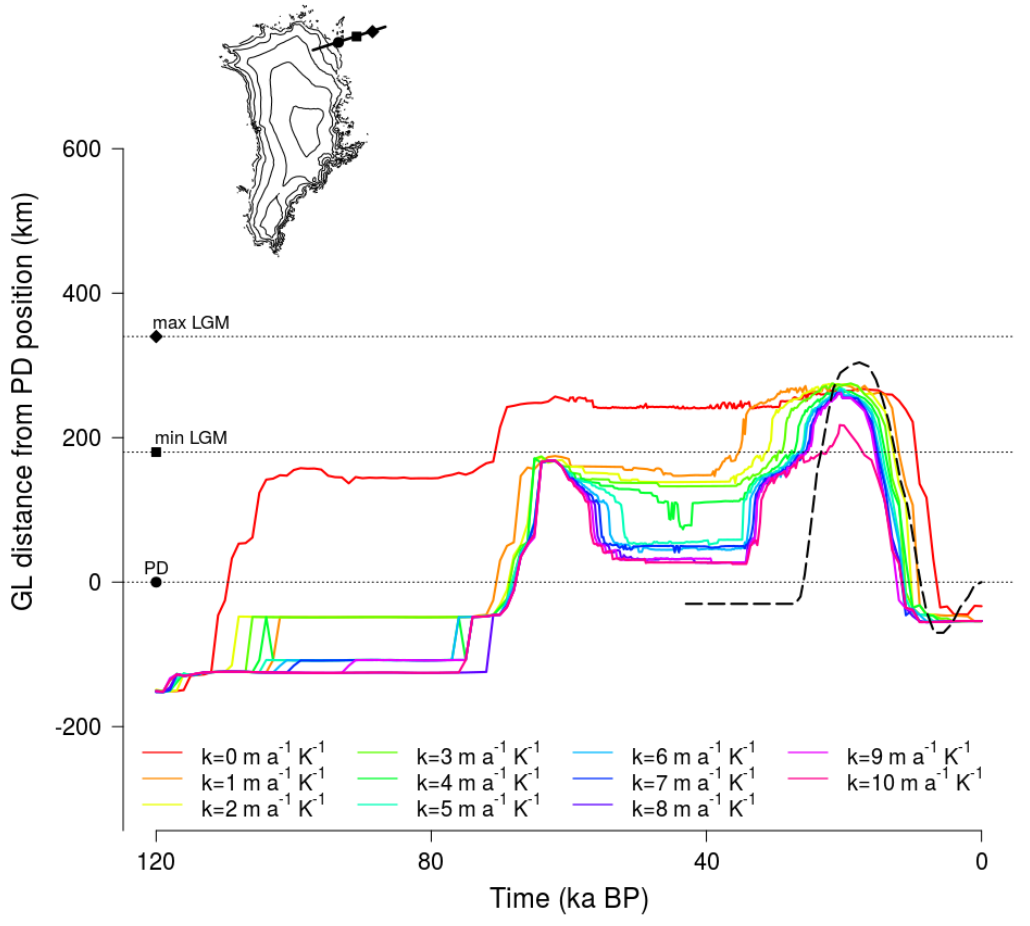

Figure 1. Evolution of the NEGIS grounding line relative to its observed present-day position for the set of experiments. The grounding-line distance has been calculated along a transect which follows approximately the flow direction of NEGIS terminating-glaciers (top-left figure of the panel). Dashed black line shows the reconstruction by Larsen et al. (2018). The black points on the GrIS figure (circle, square and diamond) show the PD NEGIS grounding-line position and the minimum and maximum expected advance of the ice sheet at the LGM according to Funder et al. (2011).

The Cryosphere Discuss., https://doi.org/10.5194/tc-2018-228
Manuscript under review for journal The Cryosphere
Discussion started: 29 November 2018

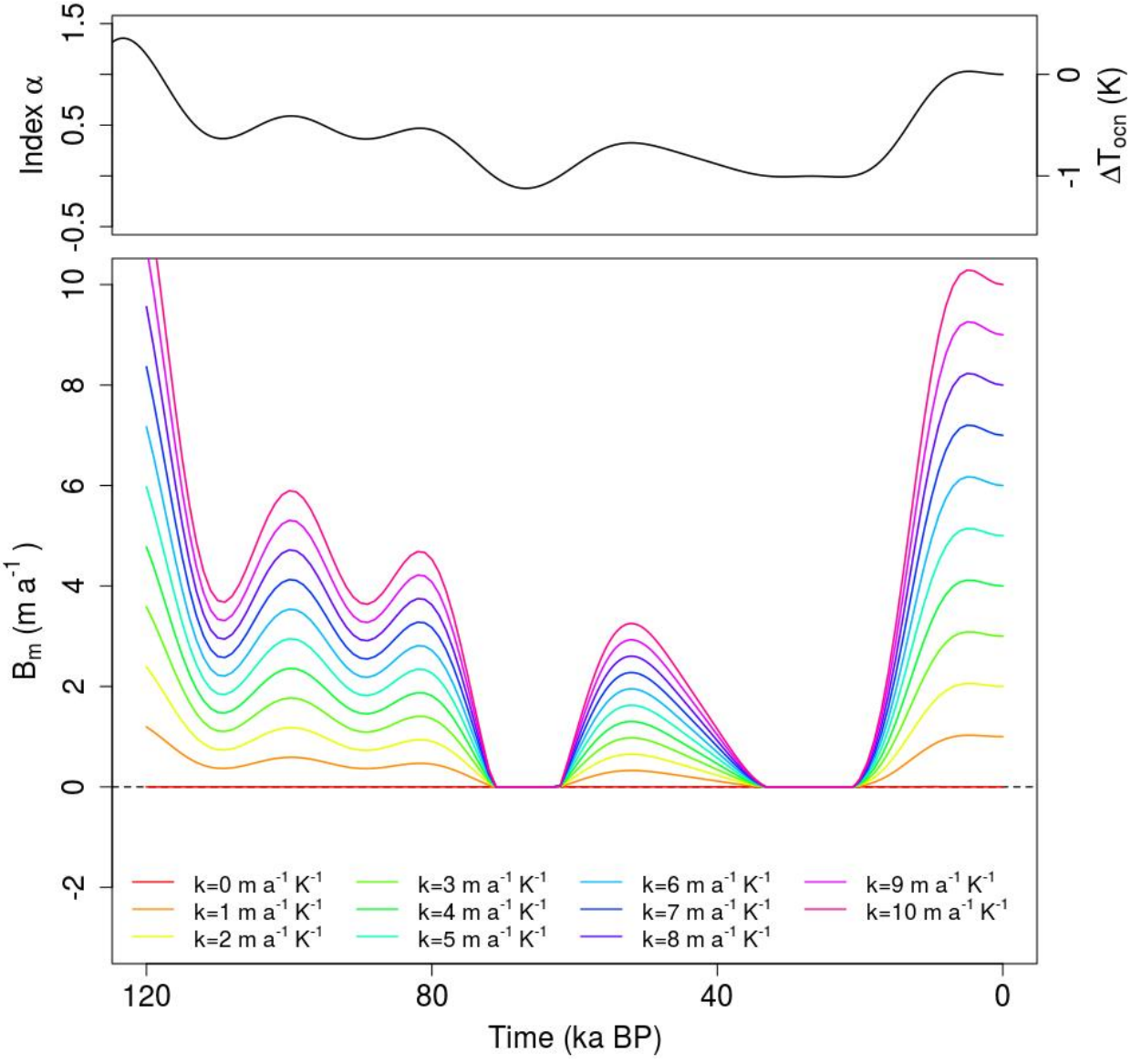

Figure 2. Evolution of the climatic index α and the resulting past oceanic temperature ΔT_{ocn} (K) (upper panel). Potential submarine melt-rate evolution during the LGP for increasing B_{ref} and κ values considered in the experiments (lower panel).

The Cryosphere Discuss., https://doi.org/10.5194/tc-2018-228
Manuscript under review for journal The Cryosphere
Discussion started: 29 November 2018

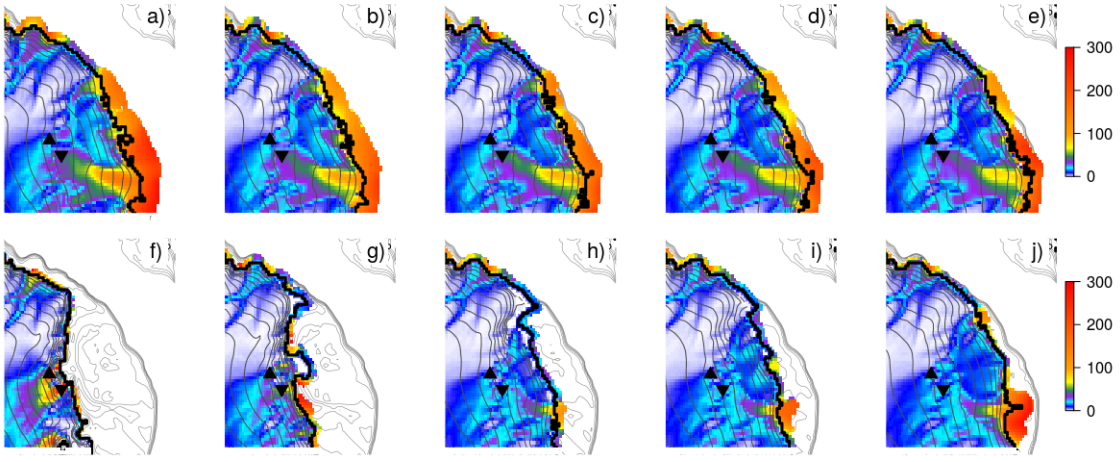

Figure 3. Snapshots of U ($m\ a^{-1}$) in total absence of submarine melting (a-e) and in presence of active orbital-driven oceanic forcing ($\kappa = 8\ m\ a^{-1}\ K^{-1}$, $B_{\mathrm{ref}} = 8m\ a^{-1}$) (f-j) at different times along MIS-3 and the LGM. Grey contour lines stands for ice surface elevation (every 250 m, superimposed to the ice sheet) and bathymetry (from 0 to -800 m, every 100 m). The black line represents the position of the simulated grounding line. PD grounding-line positions of the two main outlet glaciers of the NEGIS, Nioghalvfjerdsfjord Gletscher (NG, black up-pointing triangle) and Zachariae Isstrøm (ZI, black down-pointing triangle), are shown on the maps.

The Cryosphere Discuss., https://doi.org/10.5194/tc-2018-228
Manuscript under review for journal The Cryosphere
Discussion started: 29 November 2018

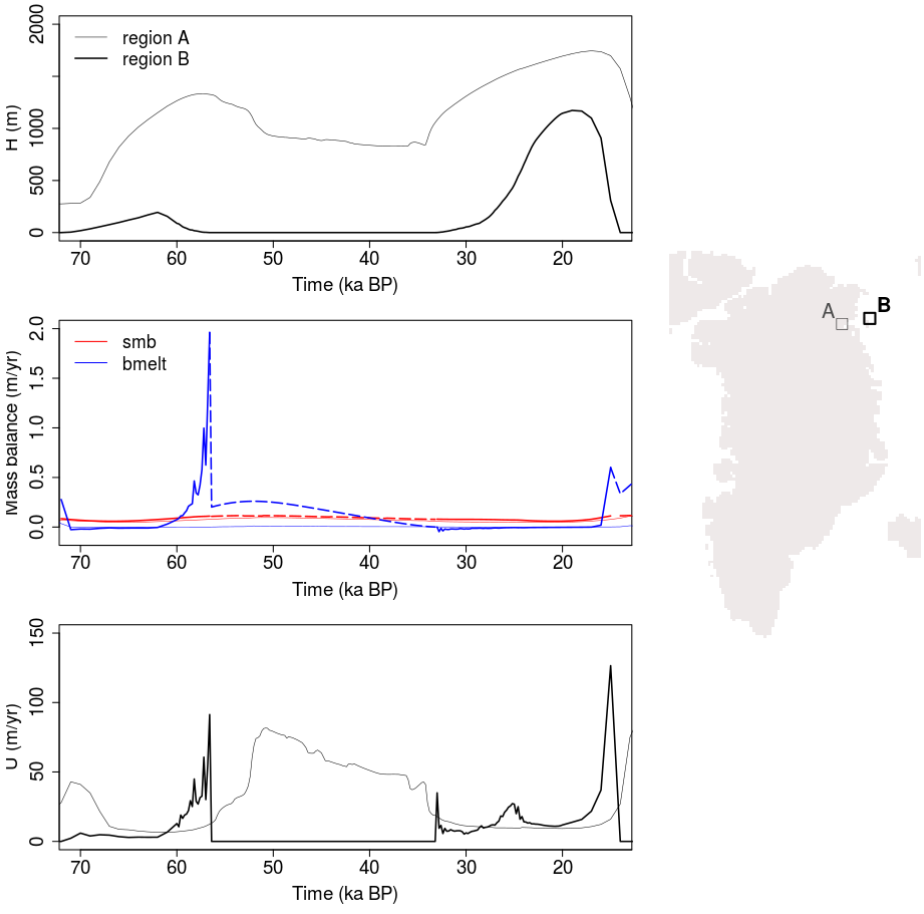

Figure 4. Time series of the averaged ice thickness H (in m), mass balance components (surface mass balance and submarine melt, both in $m\ a^{-1}$) and U ($m\ a^{-1}$) within the areas indicated in the subset, including the PD grounding-line position (thin lines, region A) and far offshore in the continental shelf (thick lines, region B) in the presence of orbitally-driven submarine melt during MIS-3 ($\kappa = 8\ m\ a^{-1}\ K^{-1}$). For mass balance, red and blue lines show the contribution to mass balance from surface mass balance and oceanic basal melt, respectively; dashed lines show the potential contributions that would be observed in presence of ice.